

# ECG Signal Super-resolution by Considering Reconstruction and Cardiac Arrhythmias Classification Loss

*Tsai-Min Chen, Yuan-Hong Tsai, Huan-Hsin Tseng, Jih-Yu Chen, Chih-Han Huang, Guo-Yuan Li, Chun-Yen Shen, and Yu Tsao\**

**Abstract—Objective:** With recent advances in deep learning algorithms, computer-assisted healthcare services have rapidly grown, especially for those that combine with mobile devices. Such a combination enables wearable and portable services for continuous measurements and facilitates real-time disease alarm based on physiological signals, e.g., cardiac arrhythmias (CAs) from electrocardiography (ECG). However, long-term and continuous monitoring confronts challenges arising from limitations of batteries, and the transmission bandwidth of devices. Therefore, identifying an effective way to improve ECG data transmission and storage efficiency has become an emerging topic. In this study, we proposed a deep-learning-based ECG signal super-resolution framework (termed ESRNet) to recover compressed ECG signals by considering the joint effect of signal reconstruction and CA classification accuracies. In our experiments, we downsampled the ECG signals from the CPSC 2018 dataset and subsequently evaluated the super-resolution performance by both reconstruction errors and classification accuracies. Experimental results showed that the proposed ESRNet framework can well reconstruct ECG signals from the 10-times compressed ones. Moreover, approximately half of the CA recognition accuracies were maintained within the ECG signals recovered by the ESRNet. The promising results confirm that the proposed ESRNet framework can be suitably used as a front-end process to reconstruct compressed ECG signals in real-world CA recognition scenarios.

**Index Terms—** Electrocardiography, sampling frequency, super-resolution.

## I. INTRODUCTION

In recent years, deep learning of artificial intelligence (AI) has been successfully used in medical diagnoses [1-9]. The integration of such software into a portable/wearable (P/W) device, e.g., Apple Watch for atrial fibrillation (AF) detection [10], has become a trend. However, there are certain drawbacks owing to hardware limitations; energy consumption is one of the main concerns [11-13]. For a P/W device, monitoring requires continuous sampling and interpretation of the user's data, irrespective of cloud service or local device, which may lead to unacceptable power consumption of a P/W device. In spite of their potential consequence of reduced information gain from users, reducing monitoring sources and sampling frequency are two compromising solutions to mitigate unacceptable power consumption.

Electrocardiography (ECG) is a noninvasive and inexpensive method clinically applied for monitoring heart functionality, which is widely implemented in P/W devices to collect users' physiological information [14, 15]. Owing to the natural limitation of P/W devices, monitoring sources are usually reduced to a single-lead ECG signal instead of a full 12-lead [16, 17], and sampling frequency is under sophisticated control. In our previous studies, we have provided an empirical discussion over a 12-lead source to select the most suitable single-lead ECG source in the case of AI prediction [18] and only the efficacy of the ECG sampling frequency remains unaddressed. It is known that, in general, a lower sampling frequency yields lower energy consumption accompanied with loss of information. Although there are studies regarding the sampling frequency of ECG, most of them are related to the association of heart rate variability, which is widely used as a noninvasive marker of the autonomic nervous system [19, 20]. Regarding the application of AI in direct CAs classification, our preliminary investigation found that the effects of sampling frequency differ from leads to leads (Fig. S1). To alleviate the loss of information, super-resolution (SR) may serve as a viable solution.

SR is a popular and well-studied area of interest recently [21-23]. The idea is to reconstruct the target information from low-resolution data. A common goal of SR is to recover the data from compressed or low-quality signals to facilitate better signal resolution for subsequent tasks. In particular, image SR has long been an important subject of image processing techniques in computer vision that aims at recovering high-resolution images from low-resolution images, which in turn is a challenging task owing to its mathematically ill-posed nature [24-27]. The rapid development of deep learning techniques in recent years also drives people to tackle image SR tasks. In general, deep learning-based SR algorithms basically differ from three major aspects: (1) network architectures such as convolutional layers, residual connections, recursive layers, and up-sampling layers [28-30]; (2) design of loss functions such as pixel loss, perceptual loss, or adversarial loss [26, 31, 32]; and (3) different types of learning principles and strategies [33-36]. These SR algorithms have reached the current state-of-the-art performance [37, 38], as well as they are proved useful for improving other vision tasks [24-27]. For instance, a task-driven SR can greatly enhance the accuracy of an object detector on low-resolution images, and thus creates a positive impact on vision recognition

[25]. Similarly, in signal processing, the audio SR refers to the task of increasing the sampling rate for a given low-resolution (i.e., low sampling rate) audio. Therefore, it can be considered as a subfield of the image SR. Motivated by recent advances in learning-based algorithms for speech recognition [39, 40], music generation [41, 42], and some other areas [43], significant progress has been made in audio SR via the introduction of deep learning. The key advantage here is that one is allowed to directly model raw signals in the time domain [41, 44], and effectively capture the long-term dependencies [45].

Although SR makes a leaping success in human vision, no prior studies, to the best of our knowledge, have attempted to apply the SR technique to ECG signals for CA prediction instead of signal reconstruction. In this paper, we proposed and investigated a novel deep-learning-based ECG SR framework (ESRNet) to reconstruct compressed signals to higher resolution with composite training loss. When using ESRNet as a front-end processor, the original ECG signals can be compressed to reduce both energy consumption and data size.

## II. THE PROPOSED METHOD

This study proposes an SR-based method called ESRNet, modified from a well-known architecture SRResNet [46], consisting of one convolution layer and 16 residual blocks [47], each of which contains two convolution layers with residual connections, followed by four convolution layers for both up-sampling and signal reconstruction, as shown in Figure 1. The ECG data sampled from low frequency were fed into this architecture for training under the same 10-fold cross-validation procedure. Throughout the entire training process, the model attempts to reconstruct a high-resolution ECG from a low sampling frequency. In contrast to the conventional SR task, which is merely increasing the resolution of an imaging system by minimizing the difference between the target and the reconstructed signal, we intended to consider CA classification results additionally. In light of this goal, a special loss function was designed to simultaneously optimize the ECG signal reconstruction and predictability for CAs, wherein the final reconstructed output is subsequently fed into another AI model, independently pretrained with a high-frequency sampled ECG under the same 10-fold cross-validation schema for final judgment. The customized joining loss  $L_J$  for ESRNet is defined as [Equation 1](#)

$$L_J(\hat{y}, y, \hat{z}, z) = \gamma L_R(\hat{y}, y) + (1 - \gamma) L_C(\hat{z}, z), \gamma \in [0, 1]$$

where  $L_R$  denotes the regression loss as the mean square error (MSE) between the original ECG signal  $y$  and the reconstructed one  $\hat{y}$ :

$$L_R(\hat{y}, y) = \frac{1}{M} \sum_{i=1}^M (\hat{y}_i - y_i)^2,$$

with  $M$  denoting the total number of pixels in  $y$  and  $\hat{y}$ . The categorical cross entropy (CCE) loss  $L_C$  measures the difference between the probability distribution of the ground truth

$z = (z_1, \dots, z_C) \in [0, 1]^C$  and that of predictions  $\hat{z} = (\hat{z}_1, \dots, \hat{z}_C) \in (0, 1)^C$  by

$$L_C(\hat{z}, z) = - \sum_{k=1}^C z_k \log(\hat{z}_k)$$

In our model, we let  $z = f_{judge}(y)$  and  $\hat{z} = f_{judge}(\hat{y})$  denote the CA probabilities using a (model-weight fixed) judge AI model  $f_{judge}$  such that the SR loss is determined

$$L_J(\hat{y}, y) = L_J(\hat{y}, y, f_{judge}(\hat{y}), f_{judge}(y)),$$

once the reconstructed ECG  $\hat{y}$  is generated. It is also understood that all the above losses are averaged over sample numbers for normalization during actual implementation.

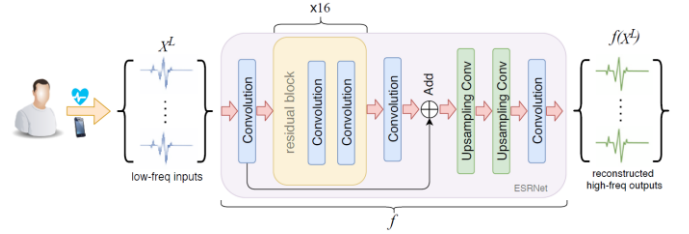


**Fig. 1. Architecture of ESRNet.** It is denoted as the function  $f$ .  $X^L$  indicates the low-frequency inputs and  $f(X^L)$  the output of the model intended to be the reconstruction of signals; layers and blocks are specified by the rectangles; “X16” indicates that 16 residual blocks are tandem-connected before joining the convolution layer.

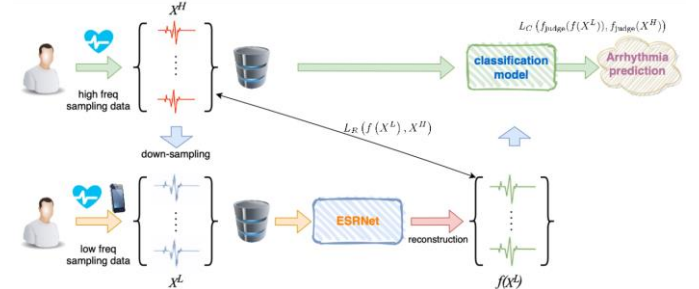


**Fig. 2. Flowchart of the proposed ESRNet for reconstruction from low sampling frequency data of single-lead ECG.** The ESRNet  $f$  receiving the low sampling frequency ECG data  $X^L$  as input generates high sampling frequency ECG prediction  $f(X^L)$  as output by considering the joint loss  $L_J$  combining the regression loss  $L_R$  and the CA classification loss  $L_C$  in Equation 1. The detailed structures of ESRNet are depicted in Fig. 1.

### III. EXPERIMENTS

In this section, we shall illustrate our experimental setting and the corresponding results.

#### A. Experimental Setup

##### 1.) F1-score

F1-score is an evaluation matrix that considers both Precision and Recall by:

$$F1 = 2 \times \frac{\text{Precision} \times \text{Recall}}{\text{Precision} + \text{Recall}},$$

$$\text{Precision} = \frac{TP}{TP + FP}, \quad \text{Recall} = \frac{TP}{TP + FN},$$

where true positive (TP), false positive (FP), true negative (TN), and false negative (FN) are defined by

$$TP_j = |\{(x_i, y_i) | y_i = f_j(x_i) = 1, 1 \leq i \leq N\}|,$$

$$FP_j = |\{(x_i, y_i) | y_i = 0 \text{ and } f_j(x_i) = 1, 1 \leq i \leq N\}|,$$

$$TN_j = |\{(x_i, y_i) | y_i = f_j(x_i) = 0, 1 \leq i \leq N\}|,$$

$$FN_j = |\{(x_i, y_i) | y_i = 1 \text{ and } f_j(x_i) = 0, 1 \leq i \leq N\}|$$

where  $(x_i, y_i)$  is the input and label of the  $i$ th sample along with the prediction from a  $C$ -category classifier  $f = (f_1, \dots, f_j, \dots, f_c) \in \{0, 1\}^c$ ; each categorical prediction  $f_j$  is binary-valued and  $|\cdot|$  measures the cardinality of a set.

##### 2.) Predictive Power Recovery

To quantify the performance recovery of the AI model by its prediction of high-frequency sampled ECGs contrasting with the low-frequency sampled ECG input received, a new evaluation metric, called predictive power recovery (PPR), is defined as follows:

$$PPR = \frac{FR - FL}{FH - FL} \leq 1$$

where FH, FL, and FR are the F1-score of the single-lead AI model in CA classification calculated by high-frequency, low-frequency sampled, and SR-reconstructed ECGs, respectively. Ideally, the relation  $FL \leq FR \leq FH \leq 1$  is expected to hold such that  $0 \leq PPR \leq 1$  with the latter equality attained when perfect reconstruction occurs. However, there exist cases where the relation fails (see Table II) and the corresponding discussions in Sec. 2.2.

##### 3.) Experimental Data

Detailed information on the CPSC2018 ECG database can be found in [48] by Liu et al. The 12-lead ECG recordings have durations from seconds to minutes; each recording has a label of nine categories including a normal type and eight abnormal CA types: AF, left bundle branch block (LBBB), right bundle branch block (RBBB), first-degree atrioventricular block (I-AVB), premature atrial contraction (PAC), premature ventricular contraction (PVC), ST-segment elevation (STE), and ST-segment depression (STD). Of the 6,877 recordings, 476 received more than one CA-type label. To simulate the measurements with low sampling frequency, the CPSC2018 open-source ECG dataset with a single CA label (6,401 out of 6,877

recordings) were downsampled from 500 Hz to 250, 125, 100, 50, 25, 15, 10, 5, and 1 Hz.

##### 4.) Bench Marked AI Network in CAs Classification

Our previous model architecture, winning CPSC 2018, was selected as the reference model to test performances at different sampling frequencies [18]. It was built on a combined architecture of five Convolutional Neural Network blocks, each containing two convolution layers and one pooling layer, followed by a bidirectional Gated Recurrent Unit [49], an attention layer [50], and finally a fully connected layer. The model has 28,035 trainable parameters so that it is compact enough to explore the statistical relations by limited computing resources.

##### 5.) 10-fold Cross-validation Procedure of Machine Learning

The data were randomly divided into 10 equal parts to set up an 8-1-1 train, validation, and test scheme of machine learning. Under such data splitting, the model was trained for 100 epochs (which refers to one complete cycle feeding training dataset) to generate 100 models (one model at each epoch), among which the one with best performance on the validation set was selected as the best model in this training process. Subsequently, this best model was used to further compute the F1-score on the test set. The procedure was repeated 10 times to complete a 10-fold training; thus, 10 best models were selected by each fold. The median F1-score for overall and each CA label, including the normal type, for the 10 test sets was calculated using the F1-score. The training process was implemented with the ADAM optimizer of the Keras package supported by TensorFlow in GPUs [51-53].

#### B. Experimental Results

In our preliminary results of ECG in CA classification among different leads and sampling frequencies, it was observed that the 25 Hz ECG sampling frequency loses most information for overall CA classification, which is contrasting to the case of 250 Hz sampling frequency that preserves the most information (Fig. S1). Based on this observation, we used our proposed SR method to recover the F1-score of the AI model from 25 Hz sampled ECG as a negative control ( $C_N$ ) to its original performance derived from 250 Hz ECG as positive control ( $C_P$ ) on the 10-fold cross-validation procedure.

##### 1.) Joint effects of two different training losses: reconstruction and classification

The loss function for the ESRNet in Equation 1 is composite and defined to optimize two distinct objectives: CCE for classification and MSE for reconstruction. Therefore, the ratio between two losses can be weighted by a constant  $\gamma \in [0,1]$ . In the following, we demonstrate three representative loss conditions: pure classification loss ( $L_C$ ), pure regression loss ( $L_R$ ), and half-mixture joint loss ( $L_J$ ), corresponding to  $\gamma = 0.0, 1.0$ , and 0.5, respectively, in Equation 1 (Fig. 3).

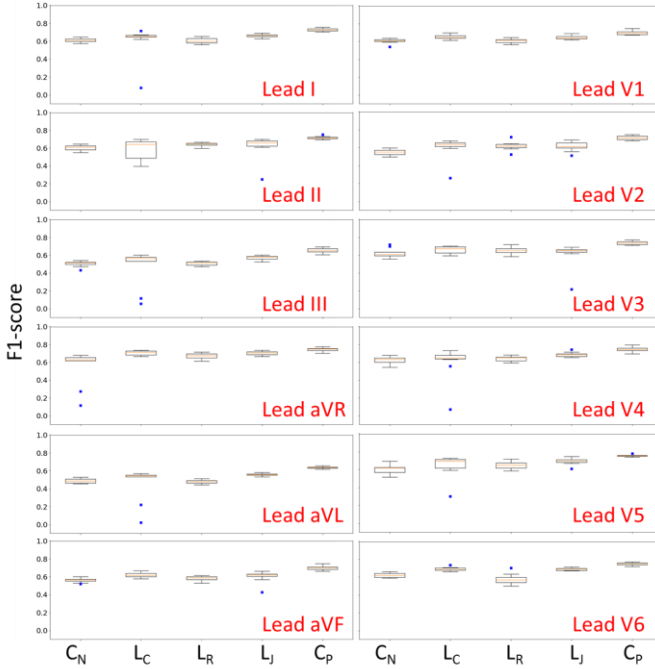


**Fig. 3. Performance comparisons of single-lead ECG model by proposed SR method with different training losses.** The overall CAs classification F1-scores of single-lead ECGs on the 10-fold cross validation derived from downsampled 25 Hz ( $C_N$ ), reconstructed 250 Hz with three different losses:  $L_C \stackrel{\text{def}}{=} L_J(\gamma = 0)$ ,  $L_R \stackrel{\text{def}}{=} L_J(\gamma = 1)$  and  $L_J \stackrel{\text{def}}{=} L_J(\gamma = 1/2)$ , and the original 250 Hz ( $C_P$ ) are shown in boxplots from left to right of each subplot. The blue dots denote the outliers beyond the interval  $[Q1 - 1.5 \cdot IQR, Q3 + 1.5 \cdot IQR]$ , where  $Q1$  and  $Q2$  are the 1st and 3rd quartiles, and  $IQR$  is the interquartile range ( $Q3 - Q1$ ).

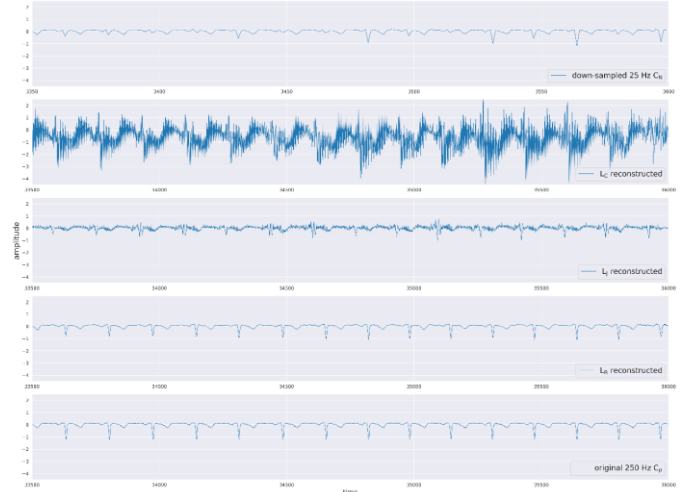
Table I shows the comparison of F1-scores of the downsampled 25 Hz data ( $C_N$ ), the original 250 Hz data ( $C_P$ ), and the reconstruction by various losses. The highest F1-score in most reconstructed CA classification tasks is achieved under  $L_J$ , except for V1, V2, and V3.

TABLE I  
OVERALL MEDIAN F1-SCORES OF DIFFERENT LOSS CONDITIONS

They are computed from the single-lead models performed on the 10-fold cross validation (see Sec. Proposed Method). The bold numbers indicate the highest scores close to their positive controls from Original 250 Hz single-lead models ( $C_P$ ).

Lead/loss	$C_N$	$L_C$	$L_R$	$L_J$	$C_P$
I	61	65	60	<b>66</b>	73
II	61	64	64	<b>66</b>	71
III	52	56	51	<b>58</b>	65
aVR	63	<b>71</b>	68	<b>71</b>	75
aVL	49	55	48	<b>56</b>	64
aVF	57	61	59	<b>62</b>	70
V1	61	<b>65</b>	62	64	69
V2	55	<b>64</b>	62	61	71
V3	61	<b>67</b>	65	65	73
V4	63	65	65	<b>68</b>	74
V5	62	<b>70</b>	65	<b>70</b>	76
V6	62	<b>69</b>	57	<b>69</b>	75

In Fig. 4, the waveforms are directly plotted to show that: (1)  $L_R$  has better reconstruction power that enables the reconstructed signals similar to the original 250 Hz signals; (2) ECG signals reconstructed by  $L_C$  may not present clear reconstruction capability. However, surprisingly, these reconstructed signals derived higher F1-scores than those reconstructed by  $L_R$  (Table I), which indicated that the comprehension of machines can sometimes be beyond human intuition; (3) ECG signals reconstructed by  $L_J$  share the characteristics of those reconstructed by  $L_C$  and  $L_R$ . These observations lead to our surmise that  $L_R$  may work as a constraint for penalty, restraining the SR model from overfitting.



**Fig. 4. ECG signals visualization of different loss conditions.** Representative ECG signals of 10-second elapse in lead II with three losses  $L_C, L_J, L_R$  are showed, where the horizontal axis has unit of time and the vertical axis indicates the ECG amplitude.

## 2.) PPRs in CAs classification by SR ECG with $L_J$

The previous results of F1 scores (Table I) have demonstrated that, in most cases,  $L_J$  can increase the CA classification accuracy along with the ECG reconstruction from low sampling frequency data. Therefore, another experiment using  $L_J$  is carried out to further investigate the reconstruction behavior of CA classification accuracy, with PPR as a new metric in different ECG leads and CAs. The results in Table II show that the PPR can reach up to overall 58%, yet variation across different leads and CAs exists.

From the color labeling in Table II, it is noted that: (1) lead aVR, V4, V5 and V6 are shown to have great potential in recovery of overall CA classification accuracy (PPR ranging from 56-58%); (2) on the contrary, lead V3 has the lowest overall PPR: 16%; (3) recovery capability of different CAs is also observed to vary from lead to lead, e.g. STE could be well recovered in lead I, II, aVR, V2, V3, V5 and V6, but III, aVL, aVF and V1. However, there exist four anomalies ( $PPR < 0$ ) in Table II, which in turn indicates that the ESRNet reconstructed signal is worse than the 25Hz downsampled frequency as  $F1(\text{reconstructed}) < F1(25\text{Hz})$ . This leads us to wonder if the reconstructed signals may have lost much information for verifying CAs.

Conventionally, in statistics, we use a t-test to confirm that two sampled populations share significant differences if their p-value is less than 0.05. Therefore, the above four anomalies

were subjected to t-test in comparison to their  $C_N$ , which are the 10-fold test F1-scores from downsampled 25 Hz. Unfortunately, none of the abnormal cases passed the criteria ( $p$ -value  $< 0.05$ ), which means that we cannot say that there are significant differences compared to  $C_N$ ; thus, we could not say there are information changes for verifying CAs in those four anomalies. Although the case of LBBB in lead V1 is intriguing with a large decrease (-125% PPR), the main reason was the extremely small differences between  $C_N$  and  $C_P$  such that  $FH - FL \approx 0$  which led to an enlarged value in  $PPR = \frac{FR - FL}{FH - FL}$  as per its definition.

Clinically, different leads provide different features of ECG for physicians and cardiologists to recognize specific types of arrhythmia [54–58]. Our experimental results in Table II show that lead V6 obtained the highest and standout PPR (98%) in LBBB among all leads, which concurs with the clinically known LBBB diagnosis criteria by distinguishing QRS morphology at leads I, aVL, V1, V2, V5, and V6 [54]. On the other hand, lead aVR also demonstrates the highest and distinguished PPRs (81%) in PVC, similar to lead V4 in STD (70% PPR) as well as lead V6 in AF (67% PPR). These are notable observations that suggest that the subtle ECG features hidden in lead aVR, V4 and V6 may serve as important judging criteria for AI models to distinguish PVC, STD, and AF, instead of human eyes.

TABLE II

MEDIAN PPRs (%) OF ESRNET 250 HZ RECONSTRUCTION BY LJ FROM 25 HZ SAMPLED DATA

Single-lead models evaluated by the 10-fold tests. The darker blue indicates the higher median PPR, with the green labeling relatively low PPR and the red labeling the anomaly PPR  $< 0$ .

CA types / Lead types	I	II	III	aVR	aVL	aVF	V1	V2	V3	V4	V5	V6
Normal	0	70	34	65	63	32	44	18	40	44	50	58
AF	38	11	36	43	47	27	48	17	0	38	55	67
I-AVB	39	55	70	42	71	58	58	85	53	68	77	65
LBBB	0	70	55	68	50	52	-125	-13	4	67	42	98
RBBB	19	41	35	54	33	61	31	-11	43	56	61	62
PAC	57	32	26	67	49	44	62	34	25	25	65	62
PVC	36	12	51	81	28	52	47	40	27	20	65	62
STD	-39	10	69	40	64	50	23	60	19	70	44	65
STE	75	97	0	106	0	0	0	105	75	33	67	54
Overall	43	40	42	57	48	43	39	47	16	56	58	57

#### IV. DISCUSSION

Collectively, AI-based ECG diagnosis of CAs has shown its feasibility and significance to improve diagnosis accuracy, compared to that of general physicians and cardiologists [59, 60]. The direct implementation of the AI model in a P/W device is becoming a trend for the future. However, there are certain limits tied to the current capability of hardware, such as battery life and computing power making it challenging to record all 12-leads ECGs at the same time for an ECG monitoring system to be implemented on a small device. A recent article suggested that an AI model built on single-lead ECG information may be able to predict CA types well enough in comparison to those based on 12 leads [18]. In respect of limitation on energy

consumption, it is to be understood that more power is required when higher frequency is used to record ECGs. Therefore, in this study, we attempted to alleviate this problem by recovering the predictive power from low sampling frequency ECG data via the proposed novel SR-based method.

For a conventional SR task, the loss function is typically merely the regression loss LR, where our experimental results also show that reconstructing ECG signals alone by LR may not always improve CA classification accuracies. Therefore, it is viable to introduce the concept of teacher–student learning by including the CCE loss from judge AI models’ output probability, as there was already a well-trained model prepared for CA classification with high-frequency ECG data [61]. Correspondingly, the experimental results suggested that the training schema by our joint loss  $L_J$  yielded better performance on CAs classification (via F1-scores) in most of the single-lead ECG data sources, with a few exceptions on lead V1, V2, and V3 (Table I). Moreover, the predictive power in the model of lead V5 trained under 250 Hz sampled ECGs achieved up to 58% of its PPR overall in the prediction of 25 Hz sampled ECGs (Table 2).

The experimental results confirm that the high-frequency structural information can be reconstructed by our ESRNet model, which leads us to consider an extension of increasing the accuracy of CA detection using the low-frequency sampled ECG data. As machine learning and AI methods continue to advance and become user-friendly, the role of ECG would gradually open up as a physiological information container. Subsequently, an AI model can be used at the right time to extract information out of the container for ignored or unattended predictions, e.g., gender and age [62]. Therefore, it is promising to expect ECG to entail more diagnostic power in many upcoming applications.

#### V. LIMITATIONS OF THE STUDY

Although our results demonstrated the predictability of each single-lead ECG from down-sampling of the CPSC2018 dataset collected from 11 hospitals in China, it is worth noticing that the predicting stability may vary from data sources, conditions, and machine types. Although the predictive power is shown to be able to approximate the high sampling frequency (250 Hz) from the low sampling frequency (25 Hz) by our SR method, it becomes more challenging when trying to recover from lower frequency signals ( $< 25$  Hz) to higher frequency signals ( $> 250$  Hz). In the absence of a systematic evaluation approach and the lack of standardized datasets as mentioned above, it becomes difficult to address these limitations at present. We consider these obstacles to be part of our future study.

## VI. SUPPLEMENTS

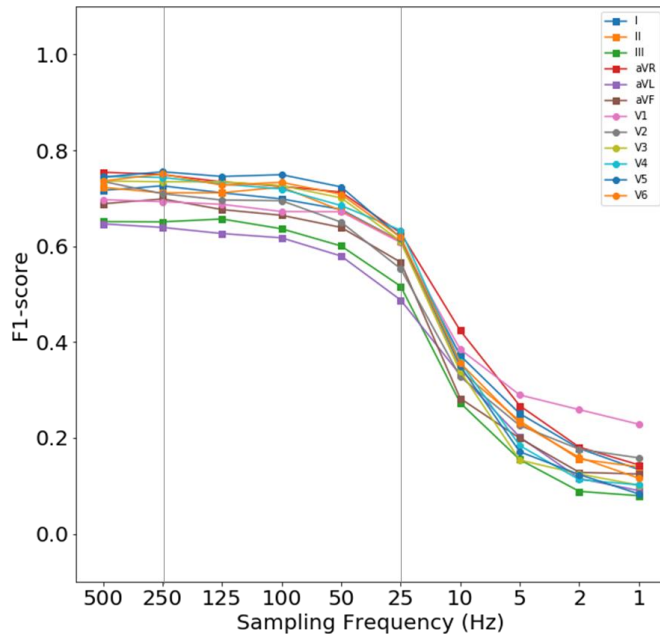


Fig. S1. The predictive power changes of single-lead ECG data through frequency down-sampling. Each line represents the median F1-score on the 10-fold tests of AI models, which are trained on single-lead ECG data, sampled from different frequencies (500, 250, 125, 100, 50, 25, 10, 5, 2, 1 Hz).

## VII. REFERENCES

- [1] A. Esteva *et al.*, "A guide to deep learning in healthcare," *Nature medicine*, vol. 25, no. 1, p. 24, 2019.
- [2] D. T. Nguyen, J. K. Kang, T. D. Pham, G. Batchuluun, and K. R. Park, "Ultrasound Image-Based Diagnosis of Malignant Thyroid Nodule Using Artificial Intelligence," *Sensors (Basel)*, vol. 20, no. 7, Mar 25 2020, doi: 10.3390/s20071822.
- [3] Y. Liu, Q. Zhang, G. Zhao, G. Liu, and Z. Liu, "Deep Learning-Based Method of Diagnosing Hyperlipidemia and Providing Diagnostic Markers Automatically," *Diabetes Metab Syndr Obes*, vol. 13, pp. 679-691, 2020, doi: 10.2147/DMSO.S242585.
- [4] S. Wang, L. Dong, X. Wang, and X. Wang, "Classification of Pathological Types of Lung Cancer from CT Images by Deep Residual Neural Networks with Transfer Learning Strategy," *Open Med (Wars)*, vol. 15, pp. 190-197, 2020, doi: 10.1515/med-2020-0028.
- [5] J. Acharya and A. Basu, "Deep Neural Network for Respiratory Sound Classification in Wearable Devices Enabled by Patient Specific Model Tuning," *IEEE Trans Biomed Circuits Syst*, Mar 18 2020, doi: 10.1109/TBCAS.2020.2981172.
- [6] L. Bishnoi and S. N. Singh, "Artificial Intelligence Techniques Used In Medical Sciences: A Review," in *2018 8th International Conference on Cloud Computing, Data Science & Engineering (Confluence)*, 11-12 Jan. 2018 2018, pp. 1-8, doi: 10.1109/CONFLUENCE.2018.8442729.
- [7] F. Gorunescu, "Intelligent decision systems in Medicine — A short survey on medical diagnosis and patient management," in *2015 E-Health and Bioengineering Conference (EHB)*, 19-21 Nov. 2015 2015, pp. 1-9, doi: 10.1109/EHB.2015.7391552.
- [8] A. Farrugia, D. Al-Jumaily, M. Al-Jumaily, A. Hussain, and D. Lamb, "Medical Diagnosis: Are Artificial Intelligence Systems Able to Diagnose the Underlying Causes of Specific Headaches?," in *2013 Sixth International Conference on Developments in eSystems Engineering*, 16-18 Dec. 2013 2013, pp. 376-382, doi: 10.1109/DeSE.2013.72.
- [9] D. Shah, G. Y. Wang, M. Dobarjeh, Z. Dobarjeh, and N. Kasabov, "Deep Learning of EEG Data in the NeuCube Brain-Inspired Spiking Neural Network Architecture for a Better Understanding of Depression," in *Gedeon T., Wong K., Lee M. (eds) Neural Information Processing*, (Lecture Notes in Computer Science. ICONIP 2019: Springer, Cham, 2019, ch. 17, pp. 195-206.
- [10] A. C. Krueger, "FDA document of Electrocardiograph software for over-the-counter use," [https://www.accessdata.fda.gov/cdrh\\_docs/pdf18/DEN180044.pdf](https://www.accessdata.fda.gov/cdrh_docs/pdf18/DEN180044.pdf) (accessed October 17, 2018).
- [11] M. Nakhkash, T. Nguyen gia, I. Azimi, A. Anzanpour, A. M. Rahmani, and P. Liljeberg, *Analysis of Performance and Energy Consumption of Wearable Devices and Mobile Gateways in IoT Applications*. 2019.
- [12] J. Kim and C. Chu, "Analysis of energy consumption for wearable ECG devices," in *SENSORS, 2014 IEEE*, 2-5 Nov. 2014 2014, pp. 962-965, doi: 10.1109/ICSENS.2014.6985162.
- [13] N. Petrellis, I.-E. Kosmadakis, M. Vardakas, F. Gioulekas, M. Birbas, and A. Lalos, "Compressing and Filtering Medical Data in a Low Cost Health Monitoring System," in *Proceedings of the 21st Pan-Hellenic Conference on Informatics*, 2017, pp. 1-5.
- [14] M. Shao, Z. Zhou, G. Bin, Y. Bai, and S. Wu, "A Wearable Electrocardiogram Telemonitoring System for Atrial Fibrillation Detection," *Sensors (Basel)*, vol. 20, no. 3, Jan 22 2020, doi: 10.3390/s20030606.
- [15] C. T. Lin *et al.*, "An intelligent telecardiology system using a wearable and wireless ECG to detect atrial fibrillation," *IEEE Trans Inf Technol Biomed*, vol. 14, no. 3, pp. 726-33, May 2010, doi: 10.1109/TITB.2010.2047401.
- [16] Apple, "Taking an ECG with the ECG app on Apple Watch Series 4," <https://support.apple.com/hr-hr/HT208955> (accessed 4/20, 2019).
- [17] L. S. Brunner, S. C. O. C. Smeltzer, B. G. Bare, J. L. Hinkle, and K. H. Cheever, *Brunner & Suddarth's Textbook of Medical-surgical Nursing* (no. 第 1 卷). Wolters Kluwer Health/Lippincott Williams & Wilkins, 2010.
- [18] T. M. Chen, C. H. Huang, E. S. C. Shih, Y. F. Hu, and M. J. Hwang, "Detection and Classification of Cardiac Arrhythmias by a Challenge-Best Deep Learning Neural Network Model," *iScience*, vol. 23, no. 3, p. 100886, Feb 4 2020, doi: 10.1016/j.isci.2020.100886.
- [19] S. Mahdiani, V. Jeyhani, M. Peltokangas, and A. Vehkaoja, "Is 50 Hz high enough ECG sampling frequency for accurate HRV analysis?," *Conf Proc IEEE Eng Med Biol Soc*, vol. 2015, pp. 5948-51, 2015, doi: 10.1109/EMBC.2015.7319746.
- [20] O. Kwon *et al.*, "Electrocardiogram Sampling Frequency Range Acceptable for Heart Rate Variability Analysis," *Healthc Inform Res*, vol. 24, no. 3, pp. 198-206, Jul 2018, doi: 10.4258/hir.2018.24.3.198.
- [21] Z. Long, T. Wang, C. You, Z. Yang, K. Wang, and J. Liu, "Terahertz image super-resolution based on a deep convolutional neural network," *Appl Opt*, vol. 58, no. 10, pp. 2731-2735, Apr 1 2019, doi: 10.1364/AO.58.002731.
- [22] M. Kwon, S. Han, K. Kim, and S. C. Jun, "Super-Resolution for Improving EEG Spatial Resolution using Deep Convolutional Neural Network-Feasibility Study," *Sensors (Basel)*, vol. 19, no. 23, Dec 3 2019, doi: 10.3390/s19235317.
- [23] K. Umehara, J. Ota, and T. Ishida, "Application of Super-Resolution Convolutional Neural Network for Enhancing Image Resolution in Chest CT," *J Digit Imaging*, vol. 31, no. 4, pp. 441-450, Aug 2018, doi: 10.1007/s10278-017-0033-z.
- [24] D. Dai, Y. Wang, Y. Chen, and L. Van Gool, "Is Image Super-resolution Helpful for Other Vision Tasks?," p. arXiv:1509.07009. [Online]. Available: <https://ui.adsabs.harvard.edu/abs/2015arXiv150907009D>
- [25] M. Haris, G. Shakhnarovich, and N. Ukita, "Task-Driven Super Resolution: Object Detection in Low-resolution Images," p. arXiv:1803.11316. [Online]. Available: <https://ui.adsabs.harvard.edu/abs/2018arXiv180311316H>
- [26] M. S. M. Sajjadi, B. Schölkopf, and M. Hirsch, "EnhanceNet: Single Image Super-Resolution Through Automated Texture Synthesis," p. arXiv:1612.07919. [Online]. Available: <https://ui.adsabs.harvard.edu/abs/2016arXiv161207919S>
- [27] Y. Bai, Y. Zhang, M. Ding, and B. Ghanem, "SOD-MTGAN: Small Object Detection via Multi-Task Generative Adversarial Network," in *Computer Vision – ECCV 2018*, Cham, V. Ferrari, M. Hebert, C. Sminchisescu, and Y. Weiss, Eds., 2018// 2018: Springer International Publishing, pp. 210-226.

- [28] W.-S. Lai, J.-B. Huang, N. Ahuja, and M.-H. Yang, "Deep Laplacian Pyramid Networks for Fast and Accurate Super-Resolution," p. arXiv:1704.03915. [Online]. Available: <https://ui.adsabs.harvard.edu/abs/2017arXiv170403915L>
- [29] C. Dong, C. C. Loy, K. He, and X. Tang, "Learning a Deep Convolutional Network for Image Super-Resolution," Cham, 2014: Springer International Publishing, in *Computer Vision – ECCV 2014*, pp. 184–199.
- [30] J. Kim, J. K. Lee, and K. M. Lee, "Accurate Image Super-Resolution Using Very Deep Convolutional Networks," p. arXiv:1511.04587. [Online]. Available: <https://ui.adsabs.harvard.edu/abs/2015arXiv151104587K>
- [31] N. Ahn, B. Kang, and K.-A. Sohn, "Fast, Accurate, and Lightweight Super-Resolution with Cascading Residual Network," p. arXiv:1803.08664. [Online]. Available: <https://ui.adsabs.harvard.edu/abs/2018arXiv180308664A>
- [32] J. Johnson, A. Alahi, and L. Fei-Fei, "Perceptual Losses for Real-Time Style Transfer and Super-Resolution," p. arXiv:1603.08155. [Online]. Available: <https://ui.adsabs.harvard.edu/abs/2016arXiv160308155J>
- [33] A. Bulat and G. Tzimiropoulos, "Super-FAN: Integrated facial landmark localization and super-resolution of real-world low resolution faces in arbitrary poses with GANs," p. arXiv:1712.02765. [Online]. Available: <https://ui.adsabs.harvard.edu/abs/2017arXiv171202765B>
- [34] C. Ledig *et al.*, "Photo-Realistic Single Image Super-Resolution Using a Generative Adversarial Network," p. arXiv:1609.04802. [Online]. Available: <https://ui.adsabs.harvard.edu/abs/2016arXiv160904802L>
- [35] B. Lim, S. Son, H. Kim, S. Nah, and K. M. Lee, "Enhanced Deep Residual Networks for Single Image Super-Resolution," p. arXiv:1707.02921. [Online]. Available: <https://ui.adsabs.harvard.edu/abs/2017arXiv170702921L>
- [36] Y. Wang, F. Perazzi, B. McWilliams, A. Sorkine-Hornung, O. Sorkine-Hornung, and C. Schroers, "A Fully Progressive Approach to Single-Image Super-Resolution," p. arXiv:1804.02900. [Online]. Available: <https://ui.adsabs.harvard.edu/abs/2018arXiv180402900W>
- [37] Y. Zhang, K. Li, K. Li, L. Wang, B. Zhong, and Y. Fu, "Image Super-Resolution Using Very Deep Residual Channel Attention Networks," p. arXiv:1807.02758. [Online]. Available: <https://ui.adsabs.harvard.edu/abs/2018arXiv180702758Z>
- [38] T. Dai, J. Cai, Y. Zhang, S. Xia, and L. Zhang, "Second-Order Attention Network for Single Image Super-Resolution," in *2019 IEEE/CVF Conference on Computer Vision and Pattern Recognition (CVPR)*, 15–20 June 2019 2019, pp. 11057–11066, doi: 10.1109/CVPR.2019.01132.
- [39] G. Hinton *et al.*, "Deep Neural Networks for Acoustic Modeling in Speech Recognition: The Shared Views of Four Research Groups," *IEEE Signal Processing Magazine*, vol. 29, no. 6, pp. 82–97, 2012, doi: 10.1109/MSP.2012.2205597.
- [40] D. Jurafsky and J. H. Martin, "Speech and language processing," (in English), 2014. [Online]. Available: <http://www.dawsonera.com/depp/reader/protected/external/AbstractView/S9781292037936>.
- [41] A. van den Oord *et al.*, "WaveNet: A Generative Model for Raw Audio," p. arXiv:1609.03499. [Online]. Available: <https://ui.adsabs.harvard.edu/abs/2016arXiv160903499V>
- [42] J.-P. Briot, G. Hadjeres, and F.-D. Pachet, "Deep Learning Techniques for Music Generation -- A Survey," p. arXiv:1709.01620. [Online]. Available: <https://ui.adsabs.harvard.edu/abs/2017arXiv170901620B>
- [43] M. A. Acevedo, C. J. Corrada-Bravo, H. Corrada-Bravo, L. J. Villanueva-Rivera, and T. M. Aide, "Automated classification of bird and amphibian calls using machine learning: A comparison of methods," *Ecological Informatics*, vol. 4, no. 4, pp. 206–214, 2009, doi: 10.1016/j.ecoinf.2009.06.005.
- [44] S. Mehri *et al.*, "SampleRNN: An Unconditional End-to-End Neural Audio Generation Model," p. arXiv:1612.07837. [Online]. Available: <https://ui.adsabs.harvard.edu/abs/2016arXiv161207837M>
- [45] S. Birnbaum, V. Kuleshov, Z. Enam, P. W. Koh, and S. Ermon, "Temporal FiLM: Capturing Long-Range Sequence Dependencies with Feature-Wise Modulations," p. arXiv:1909.06628. [Online]. Available: <https://ui.adsabs.harvard.edu/abs/2019arXiv190906628B>
- [46] C. Ledig *et al.*, "Photo-Realistic Single Image Super-Resolution Using a Generative Adversarial Network," in *2017 IEEE Conference on Computer Vision and Pattern Recognition (CVPR)*, 21–26 July 2017 2017, pp. 105–114, doi: 10.1109/CVPR.2017.19.
- [47] K. He, X. Zhang, S. Ren, and J. Sun, "Deep Residual Learning for Image Recognition," in *2016 IEEE Conference on Computer Vision and Pattern Recognition (CVPR)*, 27–30 June 2016 2016, pp. 770–778, doi: 10.1109/CVPR.2016.90.
- [48] F. Liu *et al.*, "An Open Access Database for Evaluating the Algorithms of Electrocardiogram Rhythm and Morphology Abnormality Detection," *Journal of Medical Imaging and Health Informatics*, vol. 8, no. 7, pp. 1368–1373, // 2018, doi: 10.1166/jmihi.2018.2442.
- [49] M. Schuster and K. K. Paliwal, "Bidirectional recurrent neural networks," (in English), *Ieee Transactions on Signal Processing*, vol. 45, no. 11, pp. 2673–2681, Nov 1997, doi: Doi 10.1109/78.650093.
- [50] Z. Yang, D. Yang, C. Dyer, X. He, A. J. Smola, and E. H. Hovy, "Hierarchical Attention Networks for Document Classification," in *HLT-NAACL, 2016*.
- [51] D. P. Kingma and J. Ba, "Adam: A Method for Stochastic Optimization," *ArXiv e-prints*, vol. 1412. [Online]. Available: <http://adsabs.harvard.edu/abs/2014arXiv1412.6980K>
- [52] M. Abadi *et al.*, "TensorFlow: Large-Scale Machine Learning on Heterogeneous Distributed Systems," *ArXiv e-prints*, vol. 1603. [Online]. Available: <http://adsabs.harvard.edu/abs/2016arXiv160304467A>
- [53] P. W. D. Charles, "Project Title," *GitHub repository*, vol. <https://github.com/charlespwd/project-title>, 2013.
- [54] A. B. de Luna, *Clinical Electrocardiography, Enhanced Edition: A Textbook*. Wiley, 2012.
- [55] K. Wesley, *Huszar's ECG and 12-Lead Interpretation - E-Book*. Elsevier Health Sciences, 2016.
- [56] Y. Kobayashi, "Idiopathic Ventricular Premature Contraction and Ventricular Tachycardia: Distribution of the Origin, Diagnostic Algorithm, and Catheter Ablation," *Journal of Nippon Medical School*, vol. 85, no. 2, pp. 87–94, 2018.
- [57] T. Garcia and G. Miller, *Arrhythmia Recognition: The Art of Interpretation*. Jones & Bartlett Learning, 2004.
- [58] E. B. Hanna and D. L. Glancy, "ST-segment depression and T-wave inversion: classification, differential diagnosis, and caveats," *Cleveland Clinic journal of medicine*, vol. 78, no. 6, p. 404, 2011.
- [59] A. Y. Hannun *et al.*, "Cardiologist-level arrhythmia detection and classification in ambulatory electrocardiograms using a deep neural network," *Nature medicine*, vol. 25, no. 1, p. 65, 2019.
- [60] A. Shiyovich, A. Wolak, L. Yacobovich, A. Grosbard, and A. Katz, "Accuracy of diagnosing atrial flutter and atrial fibrillation from a surface electrocardiogram by hospital physicians: analysis of data from internal medicine departments," *The American journal of the medical sciences*, vol. 340, no. 4, pp. 271–275, 2010.
- [61] J. Li, M. L. Seltzer, X. Wang, R. Zhao, and Y. Gong, "Large-Scale Domain Adaptation via Teacher-Student Learning," p. arXiv:1708.05466. [Online]. Available: <https://ui.adsabs.harvard.edu/abs/2017arXiv170805466L>
- [62] Z. I. Attia *et al.*, "Age and Sex Estimation Using Artificial Intelligence From Standard 12-Lead ECGs," *Circ Arrhythm Electrophysiol*, vol. 12, no. 9, p. e007284, Sep 2019, doi: 10.1161/CIRCEP.119.007284.